Research Square

Preprints are preliminary reports that have not undergone peer review.
They should not be considered conclusive, used to inform clinical practice,
or referenced by the media as validated information.

Ecological context shapes phage efficacy under resistance and competition

Felipe Molina

fmolina@unex.es

Universidad de Extremadura

Article

Keywords: bacteriophage, phage resistance, resource competition, continuous-culture model, phage therapy, phage-mediated suppression

Posted Date: November 20th, 2026

DOI: https://doi.org/10.21203/rs.3.rs-9849261/v1

License: This work is licensed under a Creative Commons Attribution 4.0 International License.
Read Full License

Additional Declarations: No competing interests reported.

Ecological context shapes phage efficacy under resistance and competition

Felipe Molina[1*]

1 Departamento de Bioquímica y Biología Molecular y Genética, Universidad de Extremadura, Badajoz, Spain

*fmolina@unex.es

Abstract

Bacteriophages are promising precision antimicrobials, but their effects are difficult to predict because infection dynamics depend on resistance and ecological context. Here, a resource-limited phage-host-competitor model was used to examine transient dynamics, suppression duration, and population structure across broad parameter variation under continuous-culture conditions. Resistant-host fitness and phage adsorption rate emerged as the strongest predictors of population structure at 100 h, whereas burst size, latent period, and initial phage density showed weaker or more context-dependent effects. Early phage amplification was only weakly associated with phage abundance at 100 h. Although host suppression after 24 h was comparable, median suppression persisted more than twice as long in the presence of a competitor (87.5 h versus 38.5 h), indicating that community context can substantially alter the durability of phage-mediated control even when early treatment responses appear similar. Variance-based sensitivity analysis confirmed the importance of resistant-host fitness and adsorption rate while also identifying contributions from washout rate, susceptible-host growth, and parameter interactions. The association between resistant-host fitness and population outcomes persisted under resistance reversion and competition between resistant classes but weakened when resistance permitted continued phage adsorption. These results indicate that durable phage-mediated suppression depends on resistance mechanism and ecological context as well as infection traits.

Keywords: bacteriophage; phage resistance; resource competition; continuous-culture model; phage therapy; phage-mediated suppression

Introduction

Bacteriophages are being revisited as precision antimicrobials and as alternatives or complements to antibiotics in response to rising antimicrobial resistance, driving renewed clinical and translational interest (Ganeshan and Hosseinidoust, 2019; Malik et al., 2025; Moon et al., 2025; Sahoo and Meshram, 2024). However, treatment outcomes remain difficult to predict because phage–bacteria interactions unfold within ecological contexts in which resistance, population dynamics, and interactions with other microbes jointly shape infection trajectories over time (Alkhalil, 2023; Sheraz et al., 2025; Naderian et al., 2025). As a result, phage therapy is increasingly viewed not simply as targeted killing but as an ecological perturbation with broader system-level consequences (Davies et al., 2024; Kurilovich and Geva Zatorsky, 2025). Consistent with this perspective, phage-mediated modulation of microbial communities has been explored across host-associated and environmental systems, where phage–host interactions can alter community composition, metabolic activity, and pathogen dynamics (Fujimoto, 2023; Liu et al., 2025; Xia et al., 2025; Ye et al., 2024).

Host physiological state strongly influences infection dynamics by affecting adsorption, replication timing, and phage production (Nabergoj et al., 2017; Šivec and Podgornik, 2020). Chemostat experiments have shown that lysis and phage production rates shift systematically with bacterial growth state (Bohannan and Lenski, 1997; Middelboe, 2000), providing a mechanistic basis for context-dependent infection outcomes. Under these conditions, even minor differences in initial states can decisively determine whether phages persist or are lost, despite otherwise similar parameter values (Weitz and Dushoff, 2008). Consequently, the effects of adsorption rate, latent period, burst size, and initial phage density cannot necessarily be interpreted independently of host growth and resource availability.

Resistance further complicates prediction by linking infection dynamics to evolutionary change. Resistance can arise rapidly, and its fitness consequences can reshape host-phage dynamics and long-term population outcomes (Cazares et al., 2020; Lv et al., 2026). Moreover, phage-mediated selection interacts with broader ecological constraints, allowing costly resistance to persist under specific conditions (Ruan et al., 2025). Together, these processes reduce the predictive value of individual infection traits and highlight the need for frameworks that integrate infection processes, population dynamics, and resistance evolution (Summers and Kreft, 2022). Consistent with this complexity, *in*

vitro infectivity does not always translate into *in vivo* efficacy, and baseline susceptibility alone may be insufficient to predict therapeutic success (Henry et al., 2013; Aslam et al., 2024).

Community context adds an additional layer of complexity by embedding host–phage interactions within multispecies systems. Host specificity and cophylogenetic structure indicate that susceptibility depends strongly on ecological setting (Feng et al., 2024), while expanding phage resources highlight the diversity of host–phage relationships relevant for microbiome-targeted interventions (Xing et al., 2025). Accordingly, phage-based strategies are increasingly explored for microbiome modulation, emphasizing the need to understand the ecological consequences of infection dynamics (Pottie et al., 2024). Even when infection is highly host specific, its effects can propagate indirectly through shared resources and competition, reshaping community composition without direct interaction with non-susceptible taxa (Bohannan and Lenski, 2000; Alseth et al., 2024). Experimental and natural systems likewise show that phage–host interactions can generate complex population dynamics even in simple environments, where indirect effects and ecological context determine outcomes (Chao et al., 1977; Chaïb et al., 2022; Rubio-Portillo et al., 2025). These dynamics occur within ongoing coevolutionary processes that produce context-dependent outcomes (Weitz et al., 2005), while local adaptation, host-range trade-offs, and graded infectivity further limit generalization across systems (Molina et al., 2020; Molina et al., 2025). More broadly, environmental virology shows that phage dynamics are embedded within coupled virus–host–environment systems, in which abiotic conditions and ecosystem structure modulate infection dynamics and community outcomes (Ghaly et al., 2024; Peng et al., 2025).

A substantial mathematical literature has examined these processes in resource-limited and continuous-culture systems. Early chemostat models coupled bacterial growth on a limiting resource with phage adsorption, infection, lysis, phage release, and population loss through dilution (Levin et al., 1977; Lenski and Levin, 1985). Subsequent work extended this framework to include susceptible and resistant bacterial populations, the emergence and selection of resistance, latent periods, burst sizes, infected-host dynamics, and competition under resource limitation (Bohannan and Lenski, 1997, 2000; Cairns et al., 2009; Han and Smith, 2012). More recent studies examined how adsorption, lysis time, and burst size shape phage competition under host limitation (Hunter and Fusco, 2022), and how lysis-time variability affects phage fitness under resource limitation (Smith et al., 2026).

The framework used here represents a well-mixed continuous-culture model in which susceptible hosts, resistant hosts and, where included, a non-susceptible competitor grow according to Monod kinetics while consuming a shared limiting nutrient. Resistance arises during susceptible-host

division and, in the baseline formulation, is complete, irreversible, and adsorption-blocking. An independently specified resistant-host growth rate allows resistance to impose either a fitness cost or benefit. Phage adsorption follows mass-action kinetics, while lysis and release occur after a fixed latent period represented through infection histories rather than an explicit infected-host compartment. Because the competitor shares the limiting resource but does not interact directly with the phage, its response reflects indirect effects mediated by host abundance and nutrient availability.

The objective was not to develop a new phage–host model structure, but to use an established resource-limited continuous-culture framework to determine how ecological outcomes vary across a systematically sampled parameter space. Adsorption rate, latent period, burst size, initial phage density, mutation rate, and resistant-host growth rate were varied in reduced phage–host and phage–host–competitor configurations. Each phage-exposed trajectory was compared with a matched phage-free counterfactual, allowing phage-specific effects to be distinguished from changes arising through resource limitation, dilution, mutation, and competition alone. Treatment effects were evaluated using suppression magnitude and duration, long-term dynamical classification, and correlation- and variance-based sensitivity analyses. Relationships involving resistant-host fitness were additionally examined under leaky resistance, reversible resistance, and competition between resistant classes with different growth rates.

The study addressed three questions: (i) which parameters are most strongly associated with population structure at 100 h; (ii) whether relationships involving resistant-host fitness persist across alternative resistance mechanisms; and (iii) how community context influences the duration and ecological consequences of phage-mediated suppression. Together, these analyses identify conditions associated with sustained host suppression, resistance-mediated recovery, and indirect effects on a non-susceptible competitor.

Results

Resistance and competition redirect phage–host dynamics

Population dynamics arise from interactions between a phage and a focal bacterial host , either in isolation or embedded within a community containing a non-susceptible competitor (Fig. 1A). Representative time-series trajectories illustrate model behaviour under selected parameter combinations (Fig. 1B–F). The host population comprises susceptible and resistant lineages, with

resistance preventing productive infection. Phages infect susceptible hosts, and infected cohorts lyse after a fixed latent period. All bacterial lineages compete for the same limiting resource.

In the reduced phage–host system, increasing infectivity via higher adsorption rate (σ), burst size (β), and/or initial phage density (ϕ_P) accelerates susceptible-host decline and promotes early phage amplification, often shifting dynamics from stable equilibria to sustained oscillations when resistance is absent (Fig.1B, C).

When resistance is allowed to emerge, resistant lineages expand and redirect the population dynamics, limiting the decline in total host density under otherwise identical conditions (Fig. 1D, E). Introducing a non-susceptible competitor further alters outcomes through indirect resource-mediated effects (Fig. 1F). Although competitors are not directly infected, phage-induced reductions in host density alter resource availability and competitive interactions, enabling competitor expansion in some parameter combinations. Together, these examples illustrate how resistance and community context can qualitatively alter phage-host dynamics and motivate a broader analysis of ecological outcomes.

Phage and bacterial trait variation spans a broad ecological outcome space

Ecological outcomes are mapped across a stratified Latin hypercube sampling (LHS) design that evenly distributes six parameters: adsorption rate (σ), burst size (β), latent period (ℓ), initial phage density (ϕ_P), mutation rate to resistance (μ), and resistant-host growth rate (ψ_R) (Fig. 2). The 108-parameter design provides broad coverage of the sampled parameter space while maintaining fixed continuous-culture conditions (Table 1). This sampling framework underpins subsequent analyses of population structure and parameter–outcome relationships (Figs. 3-4), temporal dynamics and convergence (Fig. 5), competitor-growth effects (Fig. 6), phage efficacy and suppression duration (Fig. 7), global sensitivity patterns (Fig. 8), and the robustness of resistance-fitness relationships under alternative resistance mechanisms (Fig. 9).

Resistant-host fitness and adsorption are the strongest correlates of population structure at 100 h

Across simulations in the reduced phage–host system, Spearman correlations reveal structured associations between endpoint densities and model parameters (Fig. 3A). Adsorption rate (σ), and the growth rate of resistant hosts (ψ_R) show the most consistent relationships with population outcomes.

Adsorption rate (σ) is negatively associated with phage abundance and susceptible-host density, whereas both σ and ψ_R are positively associated with resistant-host abundance (Fig. 3A). Consistent with these patterns, phage abundance covaries positively with susceptible hosts but negatively with resistant hosts (Fig. 3A, D), indicating that expansion of resistant lineages reduces susceptible-host availability and limits phage persistence.

Other canonical phage life-history traits show weaker or context-dependent associations. Initial phage density (ϕ_P, MOI), is weakly associated with population densities at 100 h despite its practical relevance to phage treatment. Burst size (β), latent period (ℓ), and mutation rate to resistance (μ) also show weak associations relative to ψ_R and σ within the sampled parameter ranges.

Density contours of susceptible and resistant host abundances reflect the distribution of simulation outcomes in state space, with contour intensity indicating the relative frequency of simulations occupying each region (Fig. 3B). These contours delineate regions corresponding to susceptible dominance, resistant proliferation, coexistence of host lineages, and net bacterial reduction. In contrast, characteristic parameter ranges associated with each regime are summarised separately (Fig. 3C). Susceptible-dominated outcomes occur within regions of low σ and low ψ_R, whereas resistant-dominated outcomes are associated with elevated ψ_R. High phage abundance is observed at high σ but low ψ_R, while coexistence spans intermediate regions where moderate σ coincides with sufficient ψ_R to prevent collapse. The overlap among these ranges shows that similar endpoint states can arise across multiple combinations of phage and host traits. These regimes may also differ in their temporal behaviour, with phage-dominated dynamics more often exhibiting oscillations under high σ and weak resistance, and coexistence or resistance-dominated outcomes tending toward more stable states.

The joint distribution of phage, susceptible host, and resistant host densities (Fig. 3D) forms gradients rather than discrete clusters, with variation in σ and ψ_R mapping smoothly onto this state space. This structure shows that system-level outcomes emerge from coordinated shifts across multiple population compartments rather than from variation in any single trait. Nonlinear analyses further identify regions where phage pressure, resistance emergence, or host growth dominate (Fig. 3E–G). High ψ_R and high σ favour resistant-host dominance, whereas lower σ supports coexistence of phage with both host types. Under low ψ_R but high σ, phage remain abundant, susceptible host variable and resistant host bacteria rare. Thus, population structure at the 100 h reporting horizon is associated primarily with resistant-host fitness and adsorption rate, whereas the remaining phage traits mainly modulate dynamics within this framework.

Community context broadens the range of phage-mediated outcomes

Introducing a non-susceptible competitor expands the system to a coupled host–phage–competitor interaction in which community outcomes reflect direct infection and indirect competition for the shared resource (Fig. 4). As in the reduced system, σ and ψ_R show the strongest associations with population composition at 100 h, whereas most other traits show weak to moderate associations (Fig. 4A).

Host–competitor outcomes form a structured continuum defined by the change in total host abundance under phage exposure (ΔH) and competitor performance relative to the host (ΔC_H; Fig. 4B). This space separates phage-driven suppression, competition-driven exclusion, host persistence, competition-dominated persistence, and an intermediate transition zone. When host abundance declines ($\Delta H > 0.1$), outcomes distinguish phage-driven suppression, where ΔC_H remains smaller than ΔH, from competition-driven exclusion, where ΔC_H exceeds ΔH and competitor dominance accompanies host loss. When the host persists ($\Delta H < -0.1$), outcomes distinguish host persistence, where the host remains dominant ($\Delta C_H < -0.1$), from competition-dominated persistence, where phage does not suppress the host but the competitor nevertheless outcompetes it ($\Delta C_H > 0.1$). Intermediate values define a transition region with weak or balanced effects.

In matched simulations, competitor invasion occurs in 79 of 108 designs with phage, compared with 0 of 108 without phage. This difference is accompanied by a mean increase of 12.89 $\log_{10}$ and a median increase of 17.06 $\log_{10}$ in competitor abundance, together with a median decline of 1.96 $\log_{10}$ in susceptible-host abundance. Under the conditions examined, these changes are consistent with phage exposure shifting the competitive balance in favour of the non-susceptible competitor.

Nonlinear and conditional analyses show that multispecies interactions broaden, but do not replace, the dominant role of resistance performance. Hoeffding's D reveals nonlinear and non-monotonic associations that differ between the full and reduced systems (Fig. 4C). ψ_R exerts a broad nonlinear influence ($D \approx 0.33$–0.51), indicating strong dependence even where monotonic associations weaken. σ also shows additional context-dependent effects ($|\rho| \approx 0.62$–0.71; Hoeffding's $D \approx 0.16$–0.24). Partial-correlation networks similarly show additional dependencies emerging in the presence of competition (Fig. 4D). In the phage–host–competitor system, ψ_R remains among the strongest predictors of resistant density, whereas adsorption rate contributes strongly to variation in phage density. Relative to the reduced system, μ and β gain additional conditional associations: μ is positively associated with resistant density and negatively associated with phage and competitor

densities, whereas β shows weaker associations with both. In the reduced phage–host system, ψ_R and σ dominate the conditional structure, mainly through associations with resistant density, susceptible-host depletion, and phage persistence. By contrast, β, ℓ, ϕ_P and μ show weaker or less consistent associations.

Projection of outcomes onto host–competitor shows that similar positions can arise from distinct endpoint population structures, including resistant-host dominance, susceptible–resistant coexistence, susceptible-host dominance, and host collapse with persistent phage (Fig. 4E; Supplementary Table 3B). High σ and high ϕ_P favour host suppression, whereas increased ψ_R and stronger competitive effects shift systems toward host persistence or competition-driven outcomes. Thus, community outcomes at 100 h reflect the combined associations of phage-mediated host regulation, resistance performance, and indirect competition for the shared resource.

Early phage amplification poorly predicts 100 h phage abundance

Densities at 24 h and 100 h are compared across ψ_R and σ gradients to distinguish transient infection dynamics from outcomes at the 100 h reporting point (Fig. 5A). Across simulations, median phage density decreases by 5.77 $\log_{10}$ units between 24 h and 100 h, whereas median total host and competitor densities increase by 1.43 and 2.35 $\log_{10}$ units, respectively. Phage density shows weak correspondence between the two time points (Spearman $\rho = 0.208$), unlike total host density, resistant-host density, and competitor–host balance, which are more temporally consistent ($\rho = 0.784$, $\rho = 0.856$, and $\rho = 0.841$, respectively).

Temporal divergence varies across parameter space. Between 24 h and 100 h, higher ψ_R is associated with greater phage decline ($\rho = -0.309$) and lower competitor gain ($\rho = -0.560$). At 100 h, mean total host density reaches 7.68 $\log_{10}$ in the highest ψ_R quartile, while mean competitor density falls to 2.78 $\log_{10}$; in the lowest quartile, competitor density remains high and competitor-host balance favours the competitor. Adsorption rate is also negatively associated with the change in phage density ($\rho = -0.516$). Under low adsorption, mean phage density declines from 6.65 $\log_{10}$ at 24 h to 6.13 log10 at 100 h, compared with approximately five log10 units under higher adsorption.

Extreme-outcome analysis further distinguishes phage amplification, host suppression, and competitor release (Fig. 5B). The lowest host density occurs under the same parameter combination at both reporting times, with $\log_{10} H = 0.0036$ at 24 h and 1.44 at 100 h; this combination includes high σ and β but low μ and ψ_R. Maximum host density at 100 h occurs at high ψ_R, whereas maximum competitor density occurs when ψ_R is lowest. Minimum competitor density occurs under several

parameter combinations at 24 h but is associated with high μ and ψ_R at 100 h. Maximum phage density does not coincide with minimum host density.

Most simulations remain unconverged at 100 h. Only 4.6–9.3% of designs meet the convergence criterion ($|\Delta \log_{10} \nu| < 0.5$ over the preceding 20 h) at 100 h, increasing to 37.0–43.5% at 500 h (Fig. 5C). Nevertheless, outcome classifications agree between 100 h and 500 h for 75–83% of designs (κ = 0.58–0.70; Fig. 5D, E). Associations involving ψ_R generally strengthen by 500 h, whereas those involving σ weaken, and the leading correlates of susceptible-host and phage densities differ between reporting horizons. Thus, the 100 h classifications retain substantial information about outcomes at 500 h despite continued population dynamics, but neither the reported densities nor their parameter associations represent asymptotic states (Supplementary Note 5; Supplementary Figs. 2-3).

Competitor growth shifts host–competitor balance

To examine how competitor growth rate modifies host–competitor outcomes under phage exposure, two additional simulation sets vary competitor growth by ±10% relative to the resistant host, while retaining the same Latin hypercube–sampled parameter combinations (Fig. 6A). Specifically, competitor growth rate is set to $\psi_C = 1.1\ \psi_R$ or $\psi_C = 0.9\ \psi_R$. Endpoint densities of phage, susceptible hosts, resistant hosts are summarized across ψ_R and adsorption gradients.

A 20% change in ψ_C has minimal impact on phage and susceptible-host densities across the examined ranges of ψ_R and σ. Sensitivity of phage density to the ψ_C / ψ_R ratio is most evident at intermediate resistant-host growth rates ($\psi_R \approx$ 0.6-0.8), whereas effects on susceptible-host density become apparent for $\psi_R \geq 0.5$. Consistent with earlier patterns (Fig. 3A, Fig. 4A), increasing σ is associated with reduced susceptible-host density and lower endpoint phage densities (Fig. 6A), indicating that host depletion can constrain continued phage replication.

Increasing ψ_R shifts host populations toward resistant dominance, with resistant density increasing and susceptible density declining. When ψ_C scales with ψ_R, competitor density also increases with ψ_R, reflecting the proportional increase in ψ_C. By contrast, when ψ_C is fixed and independent of ψ_R, competitor density correlates negatively with ψ_R (Fig. 4A). Accordingly, density differences between the $\psi_C = 1.1\,\psi_R$ and $\psi_C = 0.9\,\psi_R$ cases widen with ψ_R for both the competitor and resistant-host populations.

Competitor performance relative to the total host population shifted toward greater competitor dominance when $\psi_C > \psi_R$ and toward stronger host persistence when $\psi_C < \psi_R$ (Fig. 6B). However,

outcomes span a wide range at fixed ψ_C/ψ_R ratios. Comparisons with the relative growth-rate difference $(\psi_C - \psi_R)/\psi_C$ shows that competitors generally attain higher relative abundance when $\psi_C/\psi_R > 1$, but identical growth-rate ratios often produce divergent outcomes (Fig. 6C). Relative differences range from approximately zero to three orders of magnitude, with smaller differences occurring more frequently at lower growth rates. Overall, the ±10% perturbation in competitor growth altered host-competitor balance across ψ_R and σ gradients, although outcomes remained determined by the combined effects of resistance performance and phage-mediated suppression.

Persistence and conditionality of phage-mediated suppression

Phage efficacy, quantified relative to matched phage-free simulations, declined through time in both ecological systems but persisted substantially longer in the presence of a competitor (Fig. 7). Both systems reached a median efficacy of 3.06 $\log_{10}$ at 24 h, equivalent to an approximately 1,200-fold reduction in total host density. Despite this similar initial response, suppression persisted more than twice as long in the phage-host-competitor system. Median efficacy at 100 h was 0.009 $\log_{10}$ in the reduced phage-host system and 1.112 $\log_{10}$ in the phage-host-competitor system (95% bootstrap CI, 0.55–1.84). Median treatment duration, defined as maintenance of at least 50% host suppression, was 38.5 h and 87.5 h, respectively (Fig. 7C). At 100 h, 32.4% of reduced-system simulations remained above the efficacy threshold, compared with 62.0% of simulations in the phage-host-competitor system (Fig. 7B).

Thus, community context had little effect on early suppression but strongly influenced the persistence of phage-mediated control. Longer treatment duration was generally associated with lower resistant-host growth rate (ψ_R) and higher adsorption rate (σ), although substantial heterogeneity remained across parameter combinations (Fig. 7D). These results indicate that similar short-term treatment responses can produce markedly different outcomes at later reporting horizons and suggest that ecological interactions may influence treatment durability independently of initial efficacy.

Variance-based sensitivity analysis further identified resistant-host growth rate and adsorption rate as the strongest contributors to outcome variation while also revealing measurable effects of washout rate, susceptible-host growth rate, and parameter interactions (Fig. 8; Supplementary Note 7). For susceptible-host density, ψ_R had the largest total-order index in both ecological systems (ST = 0.92 and 0.82), followed by σ (ST = 0.27 and 0.29). For phage density, ψ_R was the leading contributor in the reduced phage-host system (ST = 0.58), whereas σ had the largest total-order index in the phage-

host-competitor system (ST = 0.61). In both systems, total-order indices exceeded first-order indices, indicating substantial interaction effects among parameters.

The strength of the relationship between resistant-host fitness and population outcomes depended on the mechanism of resistance (Fig. 9). Increasing residual adsorption under leaky resistance progressively weakened the association between ψ_R and total resistant-host density. At $\lambda = 1.0$, the Spearman correlation declined from 0.786 to 0.345 in the reduced system and from 0.818 to 0.271 in the phage-host-competitor system. Resistance invasion similarly decreased from 87.0% to 28.7% and from 62.0% to 38.9%, respectively.

By contrast, resistance reversion produced little change in the fitness-abundance relationship, even at $\nu = 0.1$. Fitness-dependent phenotype selection also remained evident under seeded competition between resistant classes (Supplementary Note 4; Supplementary Table 5). As class B growth increased from 0.3 to 0.75 h^{-1}, the proportion of designs dominated by class B increased from 0% to 6.5% in the reduced system and from 0% to 39.8% in the phage-host-competitor system. At $\psi_{R2} = 1.0$ h^{-1}, these values increased to 27.8% and 62.0%, respectively.

Together, these results indicate that the influence of resistant-host fitness is conditional on the mechanism by which resistance operates. Fitness effects remained evident under resistance reversion and competition among resistant phenotypes but weakened substantially when resistant hosts continued to adsorb phage.

Discussion

Resistant-host fitness and adsorption jointly influence ecological outcomes

Phage-bacteria interactions are often framed as systems in which phage life-history traits determine efficacy, with ecological context and evolutionary feedbacks acting as secondary modifiers. Across the examined parameter space, resistant-host fitness and adsorption rate were the strongest contributors to variation in ecological outcomes, whereas burst size, latent period, mutation rate, and inoculum size explained comparatively little variation. Their relative importance depended on the response variable considered, with resistant-host fitness contributing most strongly to host-density variation and adsorption contributing most strongly to phage-density variation (Bohannan and Lenski, 1997; Han and Smith, 2012). Outcomes varied continuously across parameter space, consistent with

ecological responses emerging from interactions among infection traits, resistance, and resource competition rather than from any single trait alone (Bohannan and Lenski, 2000; Alseth et al., 2024). This interpretation is consistent with evidence that phage efficacy depends on infection kinetics, bacterial physiological state, resistance, and ecological context rather than baseline susceptibility alone (Henry et al., 2013; Aslam et al., 2024).

Host physiology provides one source of such context dependence. Reduced lysis or viral production in slow-growing and stationary-phase hosts supports density- and state-dependent infection dynamics (Middelboe, 2000; Sillankorva et al., 2004), which can generate alternative stable states and history-dependent transitions (Weitz and Dushoff, 2008). Here, related variation arose through resistance emergence, susceptible-host depletion, resistant-lineage expansion, and competition for a shared resource.

In contrast to several empirical studies, MOI showed little predictive value for population densities at 100 h. MOI primarily influences infection establishment, whereas the metrics examined here reflect cumulative effects of host growth, phage replication, resource limitation, and competition. Consistent with this interpretation, adsorption rate had a substantially stronger influence than initial phage density, suggesting that sustained encounter rates are more important than initial inoculum for determining endpoint population structure.

Resistant-host fitness was strongly associated with sustained suppression, coexistence, and resistant-host persistence when resistance provided complete adsorption blocking, whereas adsorption remained a major determinant of phage persistence and abundance. Classical phage traits showed weaker or more context-dependent associations, consistent with resistance altering both susceptibility and competitive performance (Cazares et al., 2020; Alaaeddine et al., 2025).

Alternative resistance mechanisms identified an important boundary to this relationship. Per-division reversion produced little change in the association between resistant-host fitness and abundance, and competition between resistant classes retained fitness-dependent phenotype selection. In contrast, residual adsorption under leaky resistance progressively weakened both resistance invasion and the fitness-abundance relationship. Resistant-host fitness therefore acts as a conditional ecological constraint whose influence depends on the protection conferred by resistance.

The outcome space was largely continuous, although $\psi_R = \psi_S$ formed a sharp invasion boundary imposed by the single-resource chemostat structure (Bonachela et al., 2022). The prominence of this

boundary likely reflects the simplified ecological assumptions of the model, as additional sources of heterogeneity can alter host–phage dynamics and broaden outcome distributions (Liang et al., 2025).

Early amplification does not imply durable suppression

Early phage amplification did not reliably predict later phage abundance or community composition. Higher adsorption can accelerate infection and depletion of susceptible hosts, potentially explaining why strong early amplification is followed by greater phage loss in some regions of parameter space (Han and Smith, 2012; Roughgarden, 2026). Resistant-host fitness became more informative at later horizons, whereas amplification, host suppression, and competitor release occurred under different parameter combinations and therefore represent distinct outcome dimensions. Although classifications at 100 h remained moderately consistent with those at 500 h, many simulations remained dynamic. Consequently, these temporal patterns should not be interpreted as equilibrium behaviour or generalized beyond the conditions examined.

Matched phage-free simulations further showed that similar early suppression can produce markedly different long-term outcomes. Despite nearly identical median efficacy at 24 h, suppression persisted more than twice as long in the phage-host-competitor system, and nearly twice as many simulations remained above the 50% suppression threshold at 100 h. These findings indicate that early treatment success does not necessarily predict the duration of phage-mediated control and emphasize the importance of evaluating efficacy through time rather than at a single reporting horizon.

The presence of a competitor had little effect on early suppression but more than doubled median suppression duration, suggesting that ecological context can influence the persistence of phage-mediated control even when short-term treatment responses appear similar. Measurements performed over the first few hours or days of an experiment may therefore underestimate the contribution of community interactions to longer-term outcomes. Natural microbial populations are embedded within diverse ecological networks, whereas laboratory assays commonly employ single-host systems or simplified communities. Although the present model includes only a single competitor and should not be interpreted as a realistic representation of a microbiome, the results identify a plausible mechanism by which treatment durability may differ between simplified laboratory systems and more complex ecological settings. Community context may therefore influence phage-mediated control independently of its immediate effects on efficacy.

Burst size, latent period, and initial phage density showed limited independent associations with later population structure. Trade-offs with adsorption and host growth, together with host depletion

following rapid phage proliferation, may reduce their predictive value (Wang, 2006; Kannoly et al., 2022; Roughgarden, 2026; Elliott and Chevallereau, 2025). Similar conclusions have emerged from studies suggesting that adsorption and phage growth may be more informative than burst size or latency under resource-limited conditions (Bull et al., 2026; Blazanin et al., 2025). The weak inoculum effect observed here is therefore best interpreted as a feature of the continuously diluted, amplification-permissive conditions examined.

Community context modifies phage effects

Phage effects are shaped by nutrient conditions, spatial structure, host diversity, local adaptation, and interaction networks (Molina et al., 2020, 2025; Singh et al., 2025; Ghaly et al., 2024). Host-specific effects can also propagate indirectly through resource competition, influencing non-target populations without direct infection (Bohannan and Lenski, 2000; Alseth et al., 2024), and may alter system-level fitness (Kubota et al., 2025).

Here, phage exposure enabled competitor invasion in 79 of 108 parameter designs, whereas no invasions occurred in the matched phage-free simulations. Together, these results indicate indirect ecological coupling under shared-resource competition but do not imply that community complexity generally enhances phage efficacy.

Whether similar effects occur in natural communities remains uncertain because the present model excludes spatial structure, host diversity, and many ecological interactions. Nevertheless, phage-mediated lysis can promote biomass recycling (Fara et al., 2026), alter microbiome composition (Kurilovich and Geva-Zatorsky, 2025; Chen et al., 2025; Wheatley et al., 2025), and influence pathogen suppression, metabolism, and community resilience (Xia et al., 2025; Liu et al., 2025; Ye et al., 2024). Variation among hosts and interaction networks further constrains trait-based prediction (Khan et al., 2025; Li et al., 2025), while expanding databases continue to reveal extensive phage-host diversity across environments (Dieppa-Colón et al., 2025). These observations highlight the importance of incorporating ecological feedbacks when relevant biological constraints can be represented explicitly (Alkhalil, 2023; Kurilovich and Geva-Zatorsky, 2025).

Sensitivity, scope, and limitations

Global sensitivity analysis confirmed resistant-host growth and adsorption as leading contributors to outcome variation while also identifying measurable effects of washout, susceptible-host growth, and parameter interactions. The original Latin hypercube campaign therefore characterized a targeted trait

space, whereas the Sobol analysis assessed uncertainty across a broader range of ecological conditions. The difference between first- and total-order Sobol indices further indicates that parameter interactions contribute appreciably to outcome variation, supporting the view that phage efficacy emerges from combinations of ecological and infection processes rather than from any single trait in isolation.

The findings remain conditional on a well-mixed, chemostat-like environment. Spatial structure, biofilms, protected subpopulations, heterogeneous encounter rates, abortive infection, tolerance, compensatory evolution, multiple susceptible hosts, cross-infection, metabolite exchange, phage adaptation, and phage-phage interactions were not represented (Bürkle et al., 2025). Moreover, host and phage traits remained fixed throughout simulations, so the model captures ecological rather than adaptive dynamics. The reported parameter rankings should therefore be interpreted as properties of the modelled system and ecological assumptions examined here rather than universal predictors of phage efficacy.

Conclusion

Phage amplification, host suppression, and suppression persistence represent distinct outcome dimensions that cannot be inferred from one another. Across the ecological conditions examined, resistant-host fitness and adsorption rate were the strongest contributors to variation in system behaviour, while resistance mechanism and community context modified the magnitude and persistence of phage effects. Similar early suppression often produced markedly different outcomes at later reporting horizons, highlighting the importance of evaluating treatment efficacy through time rather than at a single endpoint. Together, these results indicate that phage efficacy emerges from interactions among infection dynamics, resistance characteristics, and ecological conditions rather than from any single trait in isolation.

Methods

Model overview

The framework describes population dynamics in a well-mixed continuous-culture system with constant nutrient inflow and dilution. It represents interactions among bacteriophages, a focal bacterial host, and, where specified, a non-susceptible competitor. The host population is partitioned into susceptible (S) and resistant (R) lineages, with total host density defined as $H = S + R$. Free phage particles (P) infect susceptible hosts, whereas resistant hosts (R) and competitors (C) are not productively infected in the baseline model. Infected hosts (I) are tracked implicitly through latency-dependent infection histories (Supplementary Note 2).

Two ecological configurations were analysed: a reduced phage-host system (S-R-P) and a phage-host-competitor system (S-R-P-C). In the latter, the competitor consumes the same limiting resource as the host but does not interact directly with phage. Consequently, any response of the competitor to phage exposure arises indirectly through phage-mediated changes in host density and resource availability.

The baseline configuration was derived from the demonstration input distributed with the published implementation (Nilsson, 2022) rather than fitted directly to a specific chemostat experiment. The provenance, empirical basis, and rationale for fixed parameter values are provided in Supplementary Note 6 and Supplementary Table 4.

Initial population densities were specified using the fixed conditions listed in Table 1, with ϕ_S, ϕ_R, ϕ_C, and ϕ_P denoting the initial densities of susceptible hosts, resistant hosts, competitors, and phages, respectively.

Population dynamics

Population loss is governed by chemostat dilution, following standard continuous-culture formulations in which washout is the dominant background loss process (Bohannan and Lenski, 1997; Smith and Thieme, 2012; Han and Smith, 2012).

The model tracks nutrient concentration (N), susceptible hosts (S), resistant hosts (R), competitors (C), and free phage particles (P). Infected hosts (I) are represented implicitly through infection-history arrays used to implement the latent period.

Bacterial growth is resource-limited and follows Monod kinetics. For any bacterial population $X \in \{S, R, C\}$, the realised growth rate is

$$g_X(N) = \psi_X \frac{N}{N + K}, \qquad (1)$$

where $\psi_X$is the maximum growth rate of population X, $g_X(N)$is the corresponding realised growth rate at nutrient concentration N, and K is the Monod half-saturation constant.

The susceptible-host population changes through growth, mutation to resistance, dilution, and phage adsorption:

$$\frac{dS}{dt} = g_S(N)S - \mu g_S(N)S - \omega S - \sigma SP, \qquad (2)$$

where μ is the mutation rate to resistance, ω is the dilution rate, and σ is the phage adsorption rate.

Resistant hosts arise through mutation from susceptible hosts, grow at the realised rate $g_R(N)$, and are removed through dilution:

$$\frac{dR}{dt} = g_R(N)R + \mu g_S(N)S - \omega R, \qquad (3)$$

The competitor population is unaffected by phage infection and changes according to

$$\frac{dC}{dt} = g_C(N)C - \omega C, \qquad (4)$$

where $g_C(N)$is the realised growth rate of the competitor population.

Nutrient dynamics are determined by inflow from the reservoir, dilution, and consumption by all bacterial populations:

$$\frac{dN}{dt} = \omega(N_{in} - N) - \varepsilon[g_S(N)S + g_R(N)R + g_C(N)C], \qquad (5)$$

where N_{in} is the nutrient concentration in the inflowing medium and ε is the nutrient-conversion coefficient.

Phage infection dynamics

Phage infections were represented using a fixed-delay formulation. The instantaneous rate of infection was

$$\lambda(t) = \sigma S(t) P(t), \qquad (6)$$

where σ is the adsorption rate.

After a latent period ℓ, infected hosts lyse and release β phages per infected cell. Phage dynamics were therefore

$$\frac{dP}{dt} = \beta I(t - \ell) - \sigma S(t) P(t) - \omega P(t), \qquad (7)$$

where I(t -ℓ) denotes the infected-host population completing the latent period at time t, β is burst size, and ω is the dilution rate.

Phage adsorption was implemented as a Poisson process, with infection histories stored across the latent period to determine the timing of lysis and phage release (Supplementary Note 2).

Resistance arises through deterministic mutation during susceptible-host division. Each susceptible division produces resistant offspring with probability μ, such that mutation supply depends jointly on susceptible-host growth and mutation rate. In the baseline model, resistance is assumed to be complete, irreversible, and adsorption-blocking. The resistant lineage is assigned an independent maximum growth rate (ψ_R), allowing resistance to impose either a fitness cost or a fitness benefit relative to susceptible hosts.

In the phage-host-competitor configuration, susceptible hosts, resistant hosts, and competitors compete for the same limiting resource. The competitor growth rate (ψ_C) is specified independently, and the competitor is not susceptible to phage infection. Consequently, phage-associated changes in competitor abundance arise indirectly through changes in host density and resource availability.

Simulation framework

Simulations were implemented in Cocktail (Nilsson et al., 2022) using an explicit Euler scheme with a fixed time step of 5 s ($\tau = 5/3600$ h). Growth, mutation, adsorption, infection, and lysis were updated sequentially at each time step, with infection-history arrays spanning the specified latent period.

Unless otherwise stated, simulations were run for 100 h. Population densities and ecological classifications recorded at 100 h were interpreted as transient system states rather than equilibrium values, because many parameter combinations remained dynamically active at that time.

To evaluate temporal stability, all simulations were extended to 500 h. Time-series behaviour was classified as stationary, damped, or oscillatory. Stationary dynamics exhibited negligible temporal variation, damped dynamics displayed transient oscillations approaching a stable state, and oscillatory dynamics maintained persistent fluctuations throughout the simulation period.

Parameter sampling

Six biological parameters were varied systematically: adsorption rate (σ), latent period (ℓ), burst size (β), initial phage density (φ_P), mutation rate to resistance (μ), and resistant-host growth rate (ψ_R). All other ecological conditions, including nutrient inflow, dilution rate, susceptible-host growth rate, and initial population densities, were held constant (Table 1).

A 108-point Latin hypercube design was generated to obtain stratified coverage of this six-dimensional parameter space (McKay et al., 1979; Deolia et al., 2026). Parameter ranges were chosen to encompass both experimentally reported and exploratory conditions. Parameter bounds, realised ranges, and provenance information are provided in Supplementary Table 4 and Supplementary Note 6.

Each parameter design was evaluated in both ecological configurations, producing matched outcomes for the reduced and competitor-inclusive systems. The resulting simulations represent a structured exploration of parameter space rather than independent biological replicates. Consequently, statistical summaries are interpreted descriptively and used to compare outcomes across parameter combinations rather than to infer properties of a broader population of biological systems.

To assess sensitivity to competitor growth, two additional simulation sets varied competitor growth rate (ψ_c) by ±10% relative to resistant-host growth rate (ψ_R), corresponding to $\psi_c = 0.9\ \psi_R$ and $\psi_c = 1.1\ \psi_R$ while all other parameters and initial conditions were held constant.

Outcome metrics and statistical analyses

Population densities were $\log_{10}$-transformed before analysis. Total host density was defined as

$$H = S + R$$

Host change was defined as

$$\Delta H = \log_{10}(H_{start}) - \log_{10}(H_{end})$$

Positive ΔH values indicate declining host abundance.

Competitor performance relative to the host was defined as

$$\Delta CH = \log_{10}(C_{end}) - \log_{10}(H_{end})$$

Positive ΔCH values indicate greater competitor density than total host density at the reporting horizon.

Parameter-outcome associations were quantified using Spearman rank correlation (ρ). Hoeffding's D was used to detect more general forms of dependence, including non-monotonic relationships. Partial correlations were used to quantify conditional associations, with network edges retained at $p < 0.05$ and $| PCorr | \geq 0.15$.

Because simulations represent a structured exploration of parameter space rather than biological replicates, p-values describe statistical support within the sampled parameter space and are not used to infer a broader population of natural systems. No conclusion is based on p-values alone.

Relationships between transient and long-term outcomes were evaluated using $\log_{10}$-transformed population densities and Spearman correlations. Uncertainty associated with mutation supply was evaluated separately using stochastic mutation simulations with five independent random seeds per parameter design (Supplementary Note 8).

Extended simulations

All 108 parameter designs in both ecological systems were extended to 500 h to assess the stability of the 100 h results.

For a population variable v, convergence at a reporting time was defined as

$$| \Delta \log_{10}(v) | < 0.5$$

over the preceding 20 h, corresponding to less than a three-fold change in abundance.

Convergence fractions were calculated at 100 h and 500 h. Outcome classes were assigned at both reporting horizons using the criteria applied in the primary analysis. Classification stability was quantified as the percentage of designs retaining the same classification and by Cohen's κ. Changes in population densities, outcome classifications, and parameter-outcome correlations between 100 h and 500 h were also evaluated.

Counterfactual analysis

For each parameter design and ecological system, a matched phage-free simulation was run with initial phage density set to zero and all other parameters and initial conditions unchanged.

Phage efficacy at time *t* was defined as

$$Efficacy(t) = \log_{10}\left[\frac{H_{no-phage}(t)}{H_{phage}(t)}\right]$$

Positive values indicate lower total host density in the phage-exposed simulation than in the matched phage-free simulation.

Effective suppression was defined as a reduction of at least 50% relative to the matched phage-free simulation, corresponding to

$$Efficacy \geq \log_{10}(2) = 0.301$$

Suppression duration (T_{eff}) was defined as the time until efficacy first fell below this threshold. Simulations remaining above the threshold at 100 h were treated as right-censored.

Efficacy trajectories were summarised using medians and interquartile ranges. A 95% bootstrap confidence interval for median efficacy at 100 h was estimated using 10,000 resamples.

Global sensitivity analysis

Global parameter importance was evaluated using Saltelli sampling and the Jansen estimator. All 11 model parameters were varied using N = 512 base samples, generating 6,656 model evaluations per ecological system. The analysis included the six parameters varied in the original Latin hypercube campaign together with five ecological parameters that were held constant in the primary simulations. These additional parameters were varied over ψ_S = 0.5–1.5 h^{-1}, ω = 0.1–0.3 h^{-1}, N_{in} = 50–200 μg mL^{-1}, K = 1–20 μg mL^{-1}, and ϕ_S = 10^5–10^7 CFU mL^{-1}.

First-order (S1) and total-order (ST) Sobol sensitivity indices were estimated for susceptible-host and phage densities. S1 quantifies the proportion of output variance attributable to a parameter acting alone, whereas ST quantifies the overall contribution of a parameter, including interactions with other parameters. Interaction effects were summarised as ST − S1. Uncertainty was estimated using 400 bootstrap resamples and reported as 95% confidence intervals.

The implementation was validated against benchmark functions with known analytical Sobol decompositions prior to application to the simulation outputs.

Alternative resistance mechanisms

The dependence of the resistance-fitness relationship on resistance mechanism was evaluated across 14 model variants, including leaky resistance, resistance reversion, and two-class competition scenarios. Under leaky resistance, resistant hosts adsorbed phage at a fraction λ of the susceptible-host adsorption rate (λ = 0.01, 0.1, 0.5, or 1.0). Reversible resistance was implemented as per-division reversion from R to S at ν = 10^{-5}, 10^{-3}, or 10^{-1}. Additional variants modelled competition between resistant classes that differed in growth rate.

All simulations were evaluated at 500 h, and resistance-fitness dependence was summarised using the Spearman correlation between ψ_R and total resistant-host density. Definitions of all variants and complete summary statistics are provided in Supplementary Note 4 and Supplementary Table 5.

Validation and reproducibility

Implementation reproducibility was assessed against all 217 published validation runs. Reproduced and reference trajectories showed high agreement, with a minimum Spearman correlation of 0.956 and a maximum median $|\Delta \log_{10}|$ of 0.021.

The computational framework used in this study, including model implementation, simulation workflows, analysis scripts, input files, source-data tables, publication figures, and documentation

required to reproduce all reported results, is publicly available through Zenodo (DOI: 10.5281/zenodo.23206507).

All software was developed in Python by the author. AI-assisted coding tools (OpenCode Zen, Big Pickle model) were used during software development to support code generation, debugging, and implementation of selected routines. All AI-generated code was reviewed, tested, validated, and, where necessary, modified by the author prior to inclusion in the final software release.

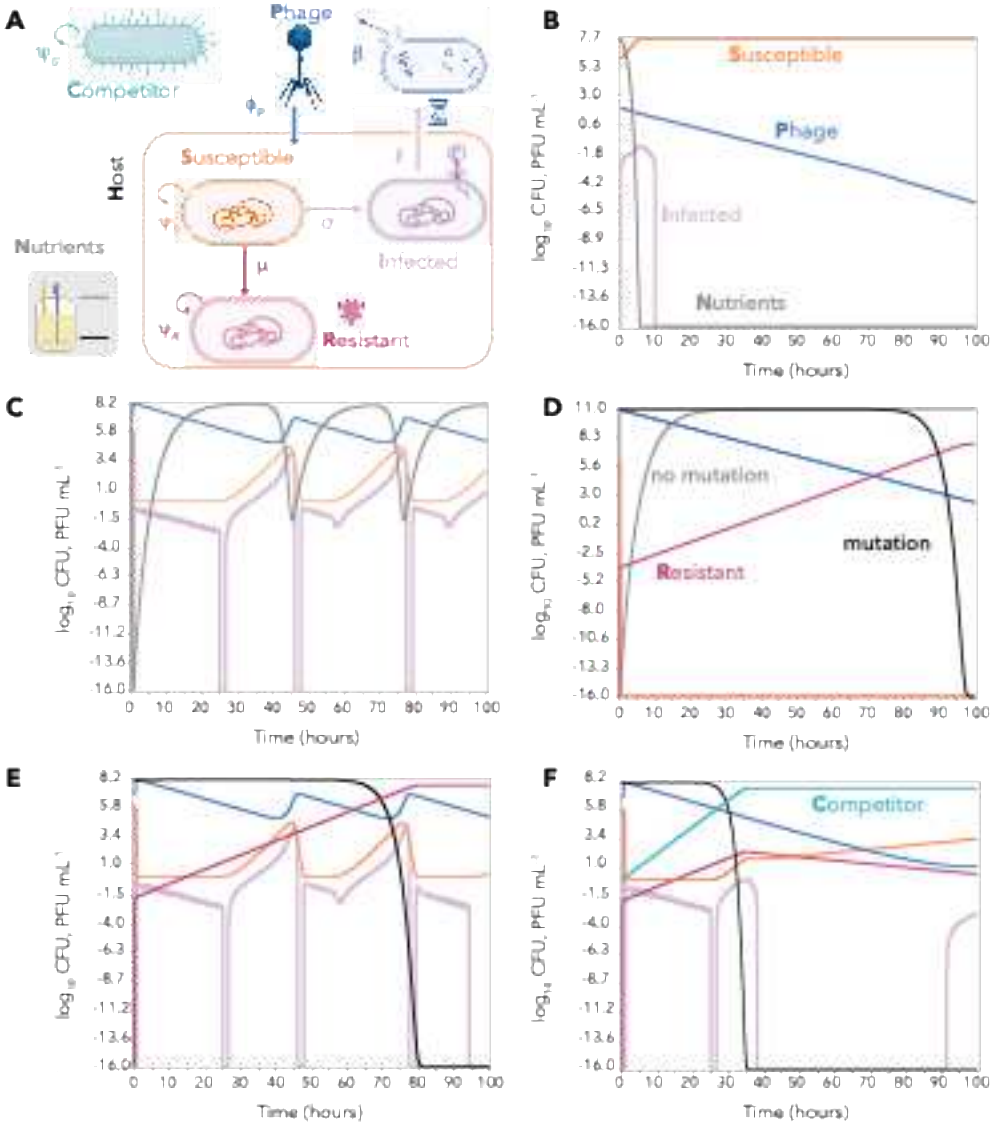


Figure 1. Resistance and competition reshape phage–host trajectories. (A) Schematic of the phage-host-competitor model. The host population consists of phage-susceptible (S), infected (I), and resistant (R) bacteria, with resistance arising by mutation during susceptible host growth. Free phage (P) infects susceptible hosts through adsorption and lysis. All bacterial populations compete indirectly through shared resource limitation; in the extended model, a competitor (C) exploits the same resource but is not susceptible to phage infection. Key phage traits – adsorption rate (σ), latent period (ℓ), burst size (β), and initial phage density (ϕ_P)– and bacterial traits–mutation rate to resistance (μ) and growth rate (ψ)– are indicated. **(B–F)** Representative time-series trajectories of phage (P), host (S, I, and R), and competitor (C) populations under representative parameter combinations, shown as $\log_{10}$-transformed densities (CFU or PFU mL^{-1}) over 100 h. **(B, C)** Systems without resistance evolution under low **(B)** and high **(C)** phage infectivity. **(D)** Comparison of trajectories with and without resistance evolution under identical phage parameters. **(E)** Resistance-enabled dynamics under high phage infectivity. **(F)** Resistance-enabled dynamics in the presence of a competing bacterial species. Parameter values are provided in Supplementary Table 1.

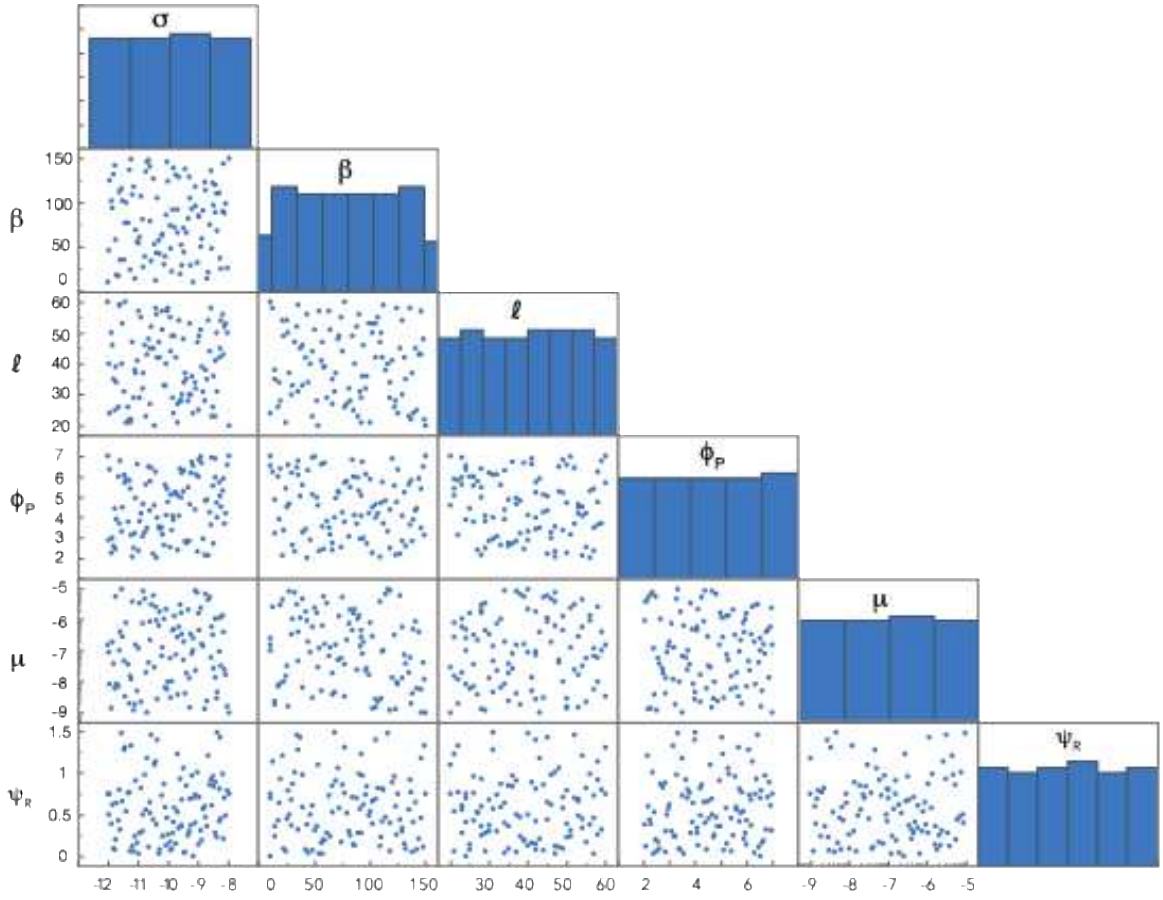
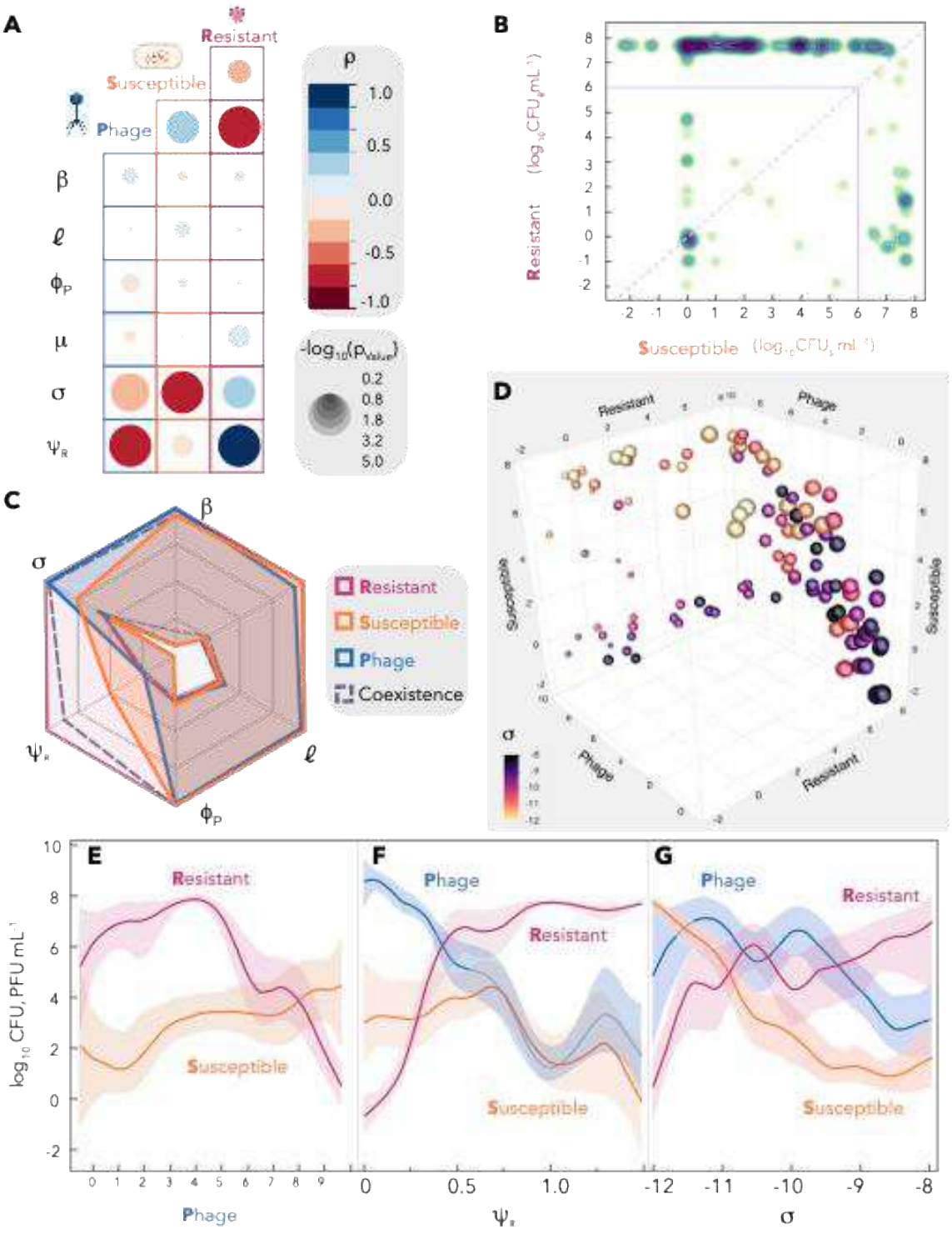


Figure 2. Stratified sampling of phage and bacterial parameters. Six model parameters were sampled using Latin hypercube stratification: phage adsorption rate (σ), burst size (β), latent period (ℓ), and initial phage density (ϕ_P), mutation rate to resistance (μ) and resistant-host growth rate (ψ_R). Parameter definitions, units, and ranges are provided in Table 1. Parameters σ, ϕ_P, and μ were sampled on a $\log_{10}$ scale. Diagonal histograms show marginal distributions, and pairwise panels show coverage of the multidimensional parameter space.

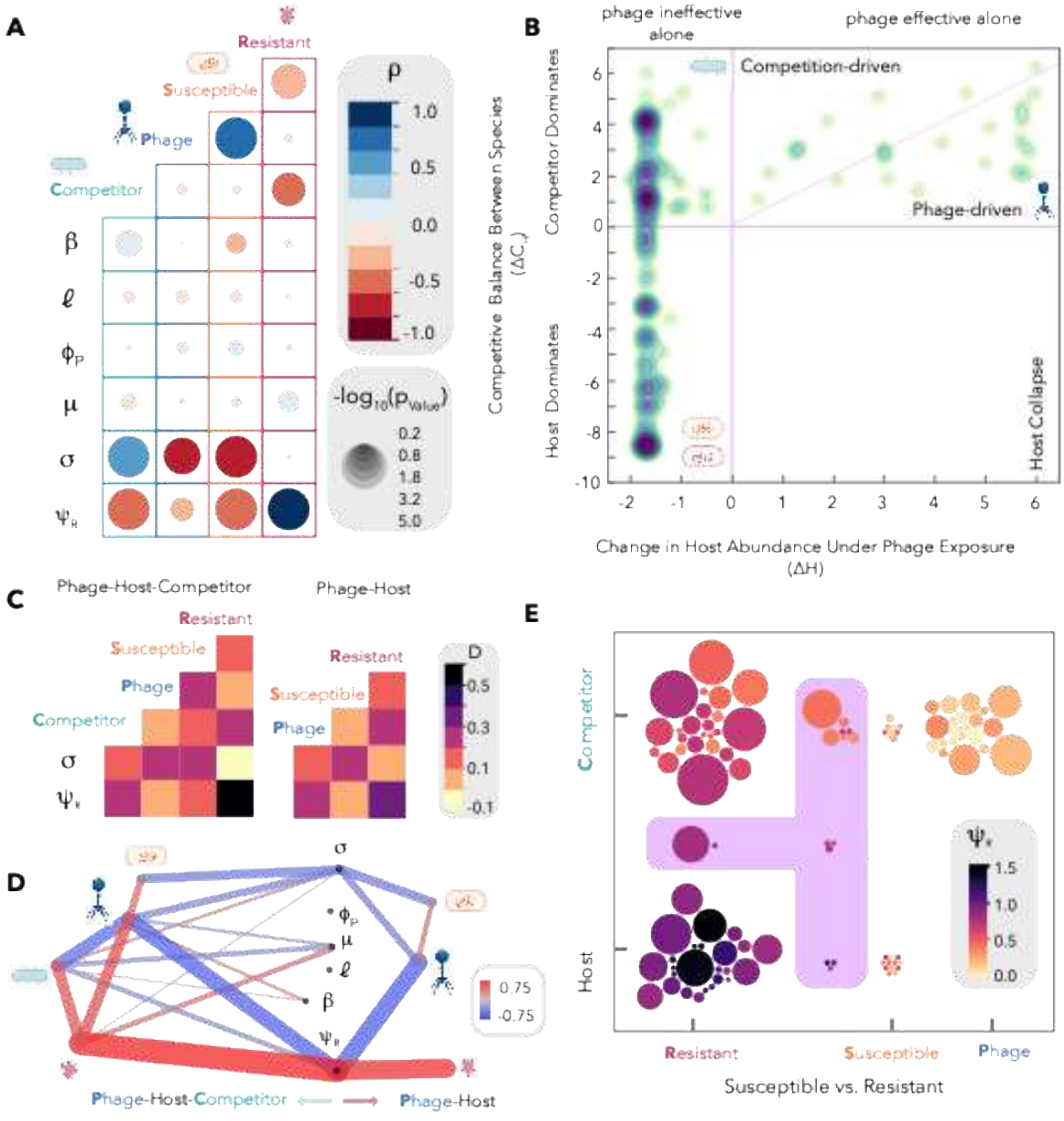

A
Resistant
Susceptible
Phage
β
ℓ
ϕ_P
μ
σ
ψ_R
ρ
1.0
0.5
0.0
-0.5
-1.0
$-\log_{10}(p_{value})$
0.2
0.8
1.8
3.2
5.0
B
Resistant ($\log_{10}$CFU$_R$mL^{-1})
Susceptible ($\log_{10}$CFU$_S$mL^{-1})
C
β
ℓ
ϕ_P
ψ_R
σ
Resistant
Susceptible
Phage
Coexistence
D
Resistant
Phage
Susceptible
σ
E
Resistant
Susceptible
$\log_{10}$CFU, PFU mL^{-1}
Phage
F
Phage
Resistant
Susceptible
ψ_R
G
Phage
Resistant
Susceptible
σ

663

664

665

Figure 3. Resistant-host fitness and adsorption are the strongest correlates of population structure at 100 h. (A) Spearman correlations between phage, susceptible-host, and resistant-host endpoint abundances and the six sampled parameters: adsorption rate (σ), latent period (ℓ), burst size (β), initial phage density (ϕ_P), mutation rate (μ), and resistant-host growth rate (ψ_R). Colour denotes correlation strength and size denotes statistical support ($-\log_{10} p$). **(B)** Density contours of susceptible and resistant host abundances ($\log_{10}$ CFU mL^{-1}) across simulations. Contour intensity indicates the relative frequency of outcomes in state space; the pink boundary denotes net bacterial reduction. **(C)** Parameter ranges associated with each ecological outcome class. Shaded regions represent the minimum and maximum values of each parameter observed within a class. **(D)** Three-dimensional distribution of phage (PFU), susceptible host (CFU), and resistant host (CFU) densities across all simulations. Each point represents a single simulation outcome, with dot color indicating the adsorption rate (σ, $\log_{10}$-scaled) and dot size reflecting the growth rate of the resistant host bacteria (ψ_R). **(E-G)** Cubic spline fits (lines) with associated confidence regions (shaded areas) summarizing how susceptible, resistant, and phage densities vary across the multidimensional parameter space. Panel **E** compares phage and bacterial densities; panel **F** shows the influence of ψ_R; and panel **G** illustrates the effect of σ.


A
Resistant
Susceptible
Phage
Competitor
β
ℓ
ϕ_P
μ
σ
ψ_R
ρ
1.0
0.5
0.0
-0.5
-1.0
$-\log_{10}(p_{Value})$
0.2
0.8
1.8
3.2
5.0
B
phage ineffective alone
phage effective alone
Competition-driven
Phage-driven
Host Collapse
Competitive Balance Between Species (ΔC_{ij})
Competitor Dominates
Host Dominates
Change in Host Abundance Under Phage Exposure (ΔH)
C
Phage-Host-Competitor
Phage-Host
D
0.5
0.3
0.1
-0.1
D
σ
ϕ_P
μ
ℓ
β
ψ_R
0.75
-0.75
Phage-Host-Competitor
Phage-Host
E
Competitor
Host
ψ_R
1.5
1.0
0.5
0.0
Resistant
Susceptible
Phage
Susceptible vs. Resistant

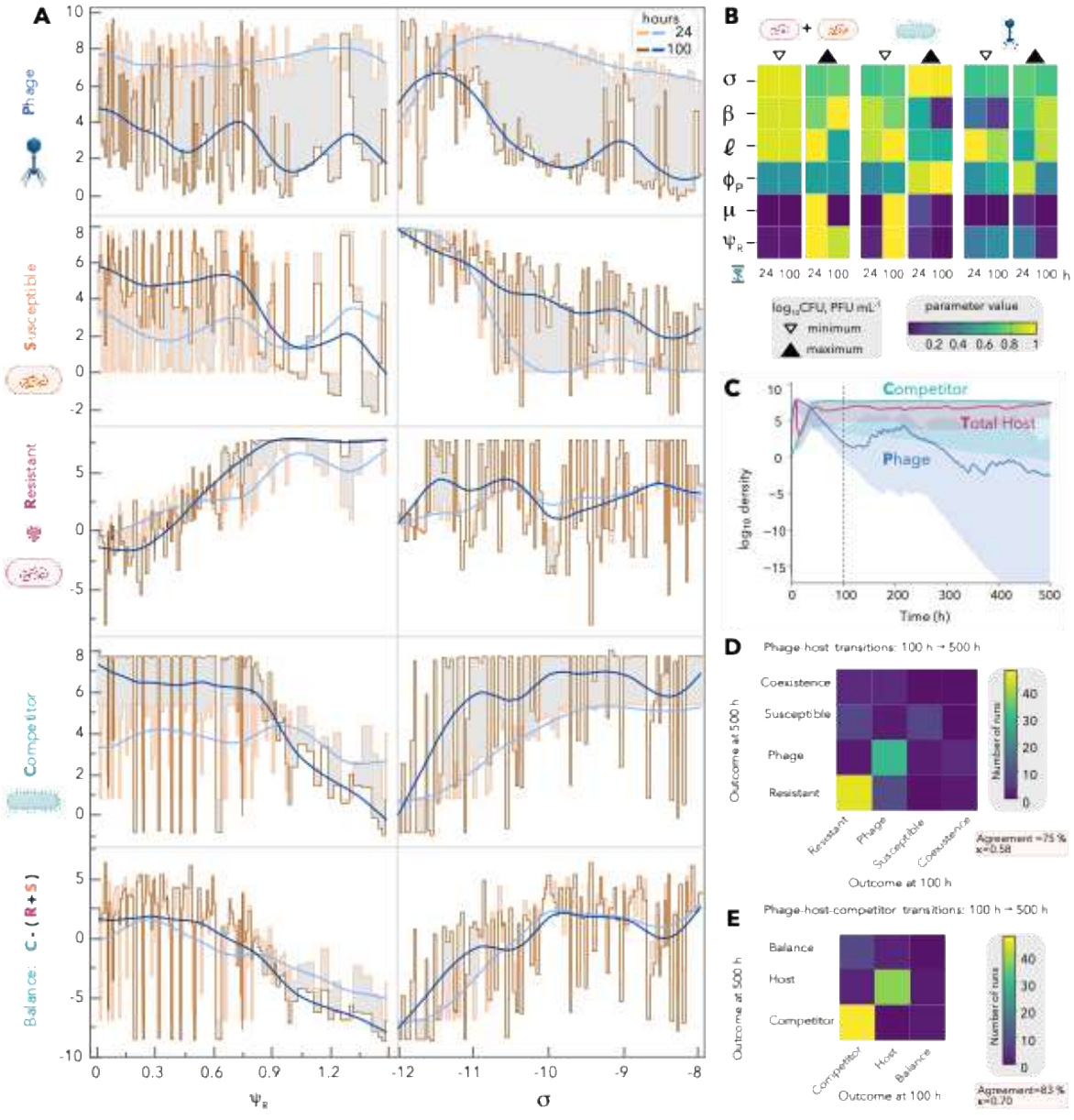
684

685

686

Figure 4. Community context broadens ecological outcomes. (A) Spearman correlations between phage and bacterial abundances and the six sampled parameters (σ, ℓ, β, ϕ_P, μ, ψ_R). Colour denotes correlation strength and size denotes statistical support ($-\log_{10} p$). **(B)** Density contours of simulation outcomes in host-competitor space. The x-axis reports the net change in total host abundance under phage exposure ($\Delta H = \log_{10} H_{start} - \log_{10} H_{end}$), where positive values indicate host decline. The y-axis shows competitor performance relative to the host ($\Delta C_H = \log_{10} C_{end} - \log_{10} H_{end}$). Within this space, four ecological regimes are distinguished. Under host decline ($\Delta H > 0.1$), outcomes separate into phage-driven host suppression, when $\Delta C_H < \Delta H$, and competition-driven exclusion, when $\Delta C_H > \Delta H$ and competitor dominance accompanies host loss. Under host persistence ($\Delta H < -0.1$), outcomes separate into host persistence, where the host remains dominant ($\Delta C_H < -0.1$), and competition-dominated persistence, where phage fails to suppress the host but the competitor nevertheless outcompetes it ($\Delta C_H > 0.1$). A central region ($|\Delta H| < 0.1$, $|\Delta C_H| < 0.1$) defines a transition zone corresponding to weak or balanced phage and competitive effects. **(C)** Heatmaps of Hoeffding's *D* values showing nonlinear and non-monotonic associations between biological parameters and endpoint abundances for the full phage–host–competitor system (left) and the reduced phage–host system (right). **(D)** Partial-correlation networks for the phage–host–competitor system (left) and the reduced phage–host system (right). Nodes represent sampled parameters and endpoint densities; edges indicate significant partial correlations ($p < 0.05$ and $|PCorr| \geq 0.15$), with edge width proportional to effect size. **(E)** Projection of outcomes onto host–competitor space showing variation in endpoint population structure. Each point represents a simulation outcome positioned according to ΔH and ΔC_H, coloured by ψ_R and scaled by σ ($\log_{10}$-scaled). Outcomes are classified by host–phage composition into resistant-host dominance, susceptible–resistant coexistence, susceptible-host dominance, and host collapse with persistent phage (Supplementary Table 3B). Pink sectors mark coexistence or non-dominance regimes.

713

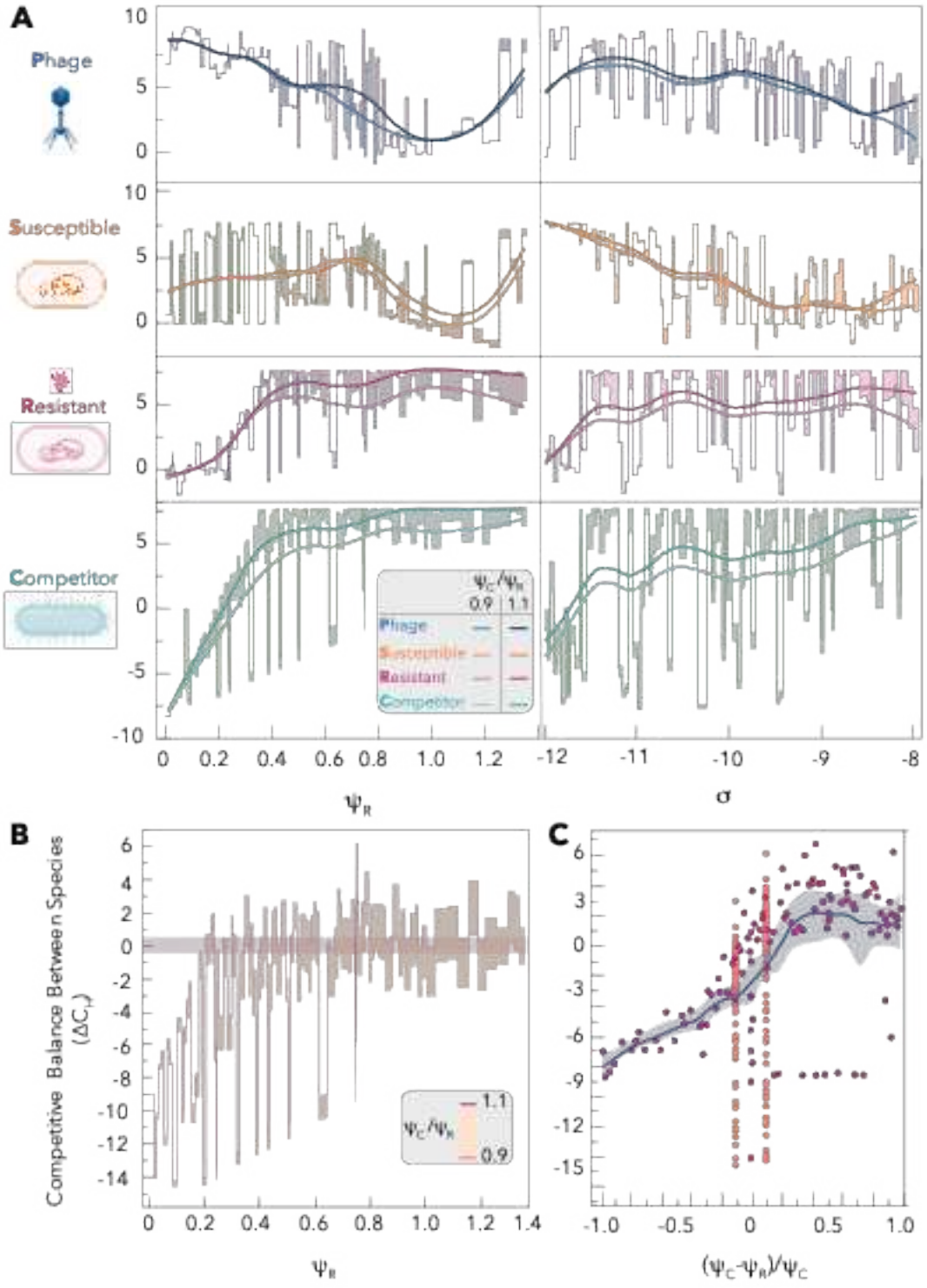

A
hours
24
100
Phage
Susceptible
Resistant
Competitor
Balance: C - (R+S)
Ψ_R
σ
B
σ
β
ℓ
Φ_P
μ
Ψ_R
24 100 24 100 24 100 24 100 24 100 24 100 h
log10CFU, PFU mL-1
minimum
maximum
parameter value
0.2 0.4 0.6 0.8 1
C
Competitor
Total Host
Phage
log10 density
Time (h)
D
Phage-host transitions: 100 h → 500 h
Coexistence
Susceptible
Phage
Resistant
Outcome at 500 h
Outcome at 100 h
Number of runs
Agreement =75 %
κ=0.58
E
Phage-host-competitor transitions: 100 h → 500 h
Balance
Host
Competitor
Outcome at 500 h
Outcome at 100 h
Number of runs
Agreement=83 %
κ=0.70

714

715

Figure 5. Early phage amplification does not reliably predict later community outcomes. (A) Comparison of $\log_{10}$-transformed population densities at 24 h and 100 h. Simulations are aggregated in binned outcome space and shown at bin centroids. Cubic-spline fits summarize trends across resistant-host growth rate (ψ_R; left x-axis) and adsorption rate (σ; right x-axis). The lower row shows competitive balance, defined as $\log_{10}(\mathrm{CFU_C}) - \log_{10}(\mathrm{CFU_H})$, where H is total host density. Positive values indicate competitor dominance and negative values indicate host dominance. **(B)** Parameter combinations associated with minimum and maximum host, competitor, and phage densities at 24 h and 100 h. Heatmap values show σ, β, ℓ, ϕ_P, μ, and ψ_R normalized to their respective maxima. **(C)** Temporal dynamics in the phage-host-competitor system extended to 500 h. Lines and shaded regions indicate medians and interquartile ranges of $\log_{10}$-transformed phage, total host, and competitor densities. The vertical dashed line marks the 100 h reporting horizon used in the primary analysis. **(D,E)** Outcome-class transitions between 100 h and 500 h in the phage-host system (D) and the phage-host-competitor system (E). Columns indicate classifications at 100 h, rows indicate classifications at 500 h, and cell values indicate the number of parameter designs assigned to each transition. *Agreement* indicates the percentage of simulations retaining the same classification between reporting horizons; κ quantifies agreement beyond that expected by chance.

736


A
Phage
Susceptible
Resistant
Competitor
10
5
0
-5
-10
0 0.2 0.4 0.6 0.8 1.0 1.2
Ψ_R
-12 -11 -10 -9 -8
σ
Ψ_C/Ψ_R
0.9 1.1
Phage
Susceptible
Resistant
Competitor
B
Competitive Balance Between Species (ΔC_i)
6 4 2 0 -2 -4 -6 -8 -10 -12 -14
0 0.2 0.4 0.6 0.8 1.0 1.2 1.4
Ψ_R
Ψ_C/Ψ_R
1.1
0.9
C
6 3 0 -3 -6 -9 -12 -15
-1.0 -0.5 0 0.5 1.0
$(\Psi_C-\Psi_R)/\Psi_C$

737

738

Figure 6. Competitor growth modulates host–competitor balance. (A) Outcomes from two additional sets of host–phage–competitor simulations using the same Latin hypercube–sampled parameter combinations, with competitor intrinsic growth rate varied relative to the resistant host. In each panel, the dark line shows the cubic-spline fit for the faster competitor ($\psi_C = 1.1\ \psi_R$), whereas the light line shows the fit for the slower competitor ($\psi_C = 0.9\ \psi_R$). Results are shown in the binned outcome space, with simulations aggregated at bin centroids. Axes report ψ_R, σ, and $\log_{10}$-transformed densities (CFU or PFU mL^{-1}; y-axis). **(B)** Competitive balance measured as $\Delta C_H = \log_{10}C_{end} - \log_{10}H_{end}$ where *H* denotes total host density (susceptible + resistant), is shown as a function of ψ_R for the two competitor-growth scenarios ($\psi_C = 1.1\ \psi_R$ and $\psi_C = 0.9\ \psi_R$) **(C)** Competitive balance is shown versus relative growth-rate difference $(\psi_C - \psi_R)/\psi_C$. Orange points correspond to the simulations in panel A; purple points correspond to the simulations in Fig. 4. Cubic-spline fit and confidence region are overlaid.

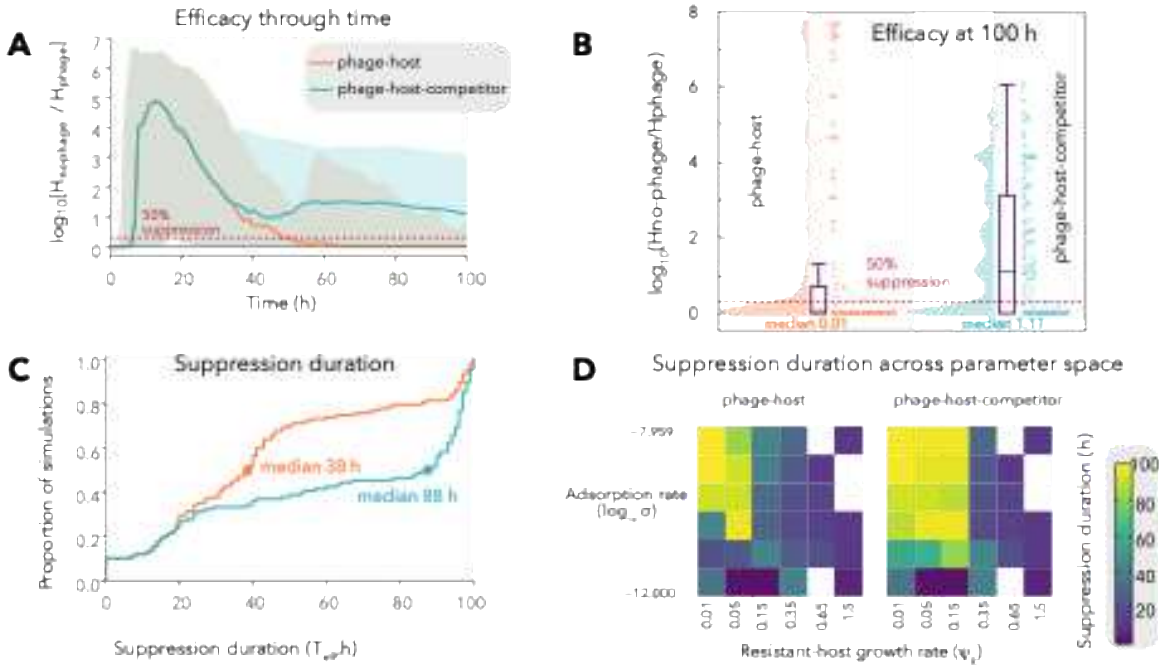


Figure 7. Ecological context influences the persistence of phage-mediated suppression. Efficacy was defined as $\log_{10}(H_{\text{no-phage}}/H_{\text{phage}})$, where H is total host density; positive values indicate host suppression relative to a matched phage-free simulation. **(A)** Efficacy through time in the phage-host and phage-host-competitor systems. Lines show medians and shaded regions indicate interquartile ranges. The red dashed line indicates the 50% suppression threshold. **(B)** Distribution of efficacy values at 100 h. Points represent individual simulations and violins show the distribution of outcomes; median values are indicated for each system. The dashed line indicates the 50% suppression threshold. **(C)** Cumulative distribution of treatment duration (T_{eff}), defined as the time until efficacy first falls below the 50% suppression threshold; simulations remaining above the threshold at 100 h were right-censored. **(D)** Median treatment duration (T_{eff}) across resistant-host growth-rate (ψ_R) and adsorption-rate (σ) bins in the phage-host system (left) and the phage-host-competitor system (right). Colour intensity indicates median treatment duration within each parameter bin.

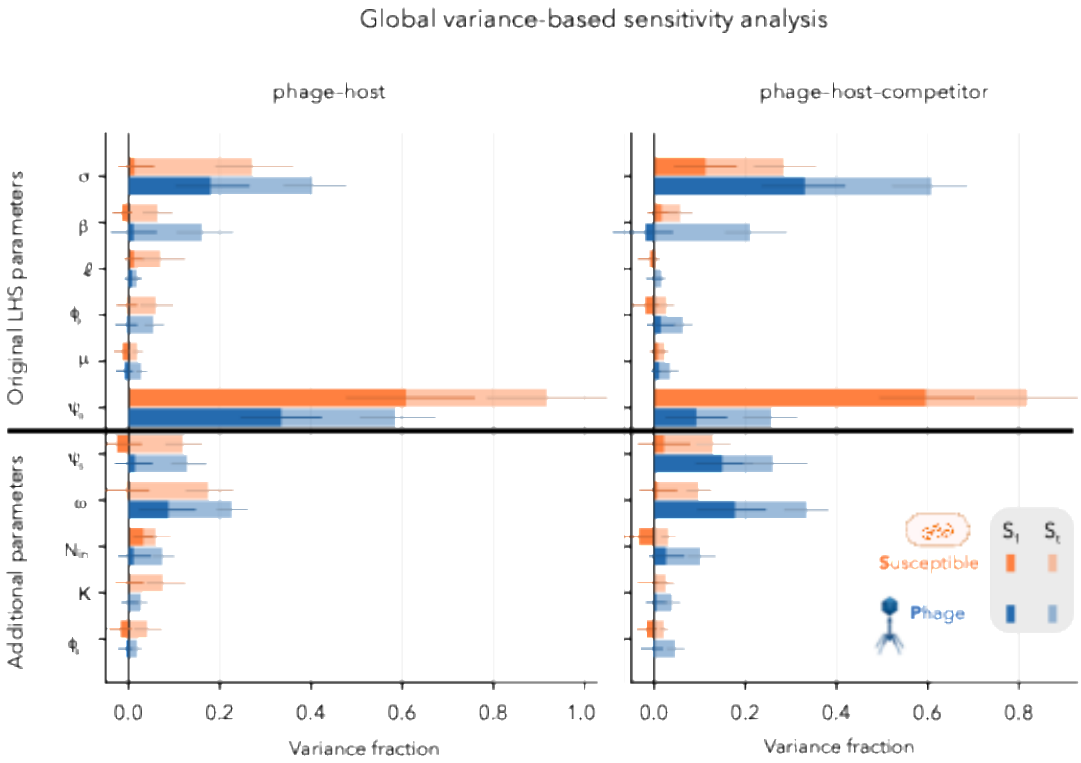


Figure 8. Global variance-based sensitivity analysis. Sobol sensitivity indices were estimated using Saltelli sampling and the Jansen estimator (N = 512 base samples). Solid and transparent bars show first-order (S1) and total-order (ST) sensitivity indices, respectively; error bars indicate 95% bootstrap confidence intervals based on 400 bootstrap resamples. Orange bars represent susceptible-host abundance (S) and blue bars represent phage abundance (P). Parameters are grouped according to whether they were included in the original Latin hypercube design or added as previously fixed ecological parameters in the expanded sensitivity analysis. The phage-host system is shown on the left and the phage-host-competitor system on the right.

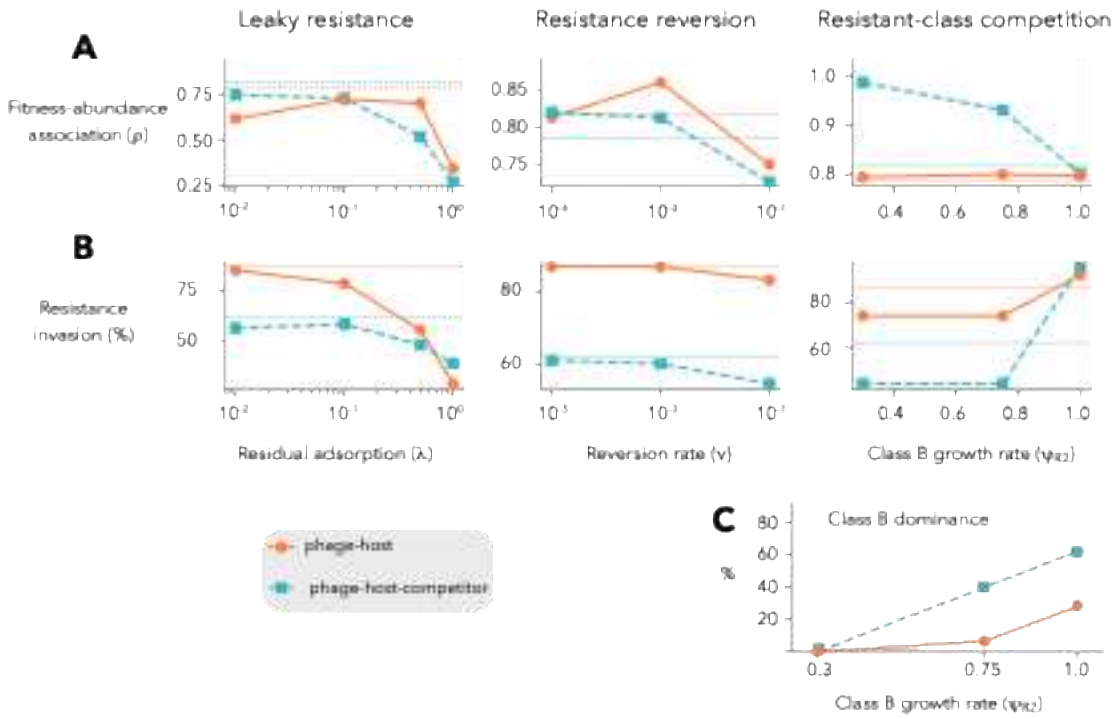


Figure 9. Effects of alternative resistance mechanisms on resistance-fitness associations. Results are shown for leaky resistance (λ), resistance reversion (ν), and competition between resistant classes with alternative ψ_{R2} values. **(A)** Association between resistant-host growth rate (ψ_R) and total resistant-host density, quantified by Spearman correlation (ρ). **(B)** Percentage of parameter designs in which resistance invades. **(C)** Percentage of parameter designs in which class B dominates the resistant population. Orange circles indicate the reduced phage-host system and blue squares indicate the phage-host-competitor system. Dotted horizontal lines indicate the corresponding complete adsorption-blocking baseline. Definitions of resistance variants and complete summary statistics are provided in Supplementary Note 4 and Supplementary Table 5.

References

1. Alaaeddine, R., Al-Mohammed, N. H., Pillai, J. & Fayyad-Kazan, M. Phage therapy for drug-resistant infections: mechanisms, evidence, and emerging clinical strategies. Mol. Biol. Rep. 52, 1051 (2025).

2. Alkhalil, S. S. The role of bacteriophages in shaping bacterial composition and diversity in the human gut. Front. Microbiol. 14 (2023).

3. Alseth, E. et al. The impact of phage and phage resistance on microbial community dynamics. PLoS Biol. 22, e3002346 (2024).

4. Aslam, S. et al. Pseudomonas aeruginosa ventricular assist device infections: findings from ineffective phage therapies in five cases. Antimicrob. Agents Chemother. 68, e01728-23 (2024).

5. Blazanin, M., Vasen, E., Jolis, C., An, W. & Turner, P. Quantifying phage infectivity from characteristics of bacterial population dynamics. Proc. Natl. Acad. Sci. U.S.A. 122, e2513377122 (2025).

6. Bohannan, B. J. M. & Lenski, R. E. Effect of resource enrichment on a chemostat community of bacteria and bacteriophage. Ecology 78, 2303–2315 (1997).

7. Bohannan, B. J. M. & Lenski, R. E. The relative importance of competition and predation varies with productivity in a model community. Am. Nat. 156, 329–340 (2000).

8. Bonachela, J. A., Choua, M. & Heath, M. R. Unconstrained coevolution of bacterial size and the latent period of plastic phage. PLoS One 17, e0268596 (2022).

9. Bull, J. J., Kaur, G. & Krone, S. M. Modeling the phage properties best for therapy. Viruses 18, 240 (2026).

10. Bürkle, M. et al. Phage-phage competition and biofilms affect interactions between two virulent bacteriophages and Pseudomonas aeruginosa. ISME J. 19, wraf065 (2025).

11. Cairns, B. J., Timms, A. R., Jansen, V. A. A., Connerton, I. F. & Payne, R. J. H. Quantitative models of in vitro bacteriophage-host dynamics and their application to phage therapy. PLoS Pathog. 5, e1000253 (2009).

12. Cazares, A., García-Contreras, R. & Pérez-Velázquez, J. Eco-evolutionary effects of bacterial cooperation on phage therapy: an unknown risk? Front. Microbiol. 11, 590294 (2020).

13. Chaïb, A. et al. Phage-host interactions as a driver of population dynamics during wine fermentation: betting on underdogs. Int. J. Food Microbiol. 383, 109936 (2022).

14. Chao, L., Levin, B. R. & Stewart, F. M. A complex community in a simple habitat: an experimental study with bacteria and phage. Ecology 58, 369–378 (1977).

15. Chen, L., Huang, Z., Middelboe, M., Deng, D. & Ma, Y. Synergistic effects of commensals and phage predation in suppressing colonization by pathogenic *Vibrio parahaemolyticus*. npj Biofilms Microbiomes 11, 163 (2025).

16. Chen, W. et al. Exploring diversity and distribution patterns of chicken gut bacteriophage community. Anim. Microbiome 7, 119 (2025).

17. Davies, T. et al. Ecological phage therapy: can bacteriophages help rapidly restore the soil microbiome? Ecol. Evol. (2024). doi:10.1002/ece3.70185.

18. Deolia, P., Singh, A. & Mubayi, A. Mathematical modeling of sequential Dengue–Zika infections: dynamic insights into antibody-dependent enhancement and neutralization effects. Sci. Rep. 16, 14872 (2026).

19. Dieppa-Colón, E., Martin, C., Kosmopoulos, J. C. & Anantharaman, K. Prophage-DB: a comprehensive database to explore diversity, distribution, and ecology of prophages. Environ. Microbiome 20, 5 (2025).

20. Elliott, J. & Chevallereau, A. Fast phages outcompete by depleting host resources. Trends Microbiol. 33, 703–704 (2025).

21. Fara, E. et al. Phage-mediated lysis increases growth rate of surviving bacterial cells. iScience 29, 115899 (2026).

22. Feng, Y. et al. Host specificity and cophylogeny in the “animal-gut bacteria-phage” tripartite system. npj Biofilms Microbiomes 10, 88 (2024).

23. Fujimoto, K. Metagenome data-based phage therapy for intestinal bacteria-mediated diseases. Biosci. Microbiota Food Health 42, 8–12 (2023).

24. Ganeshan, S. D. & Hosseinidoust, Z. Phage therapy with a focus on the human microbiota. Antibiotics 8, 131 (2019).

25. Geng, Y., Nguyen, T. V. P., Homaee, E. & Golding, I. Using bacterial population dynamics to count phages and their lysogens. Nat. Commun. 15, 7814 (2024).

26. Ghaly, T. M. et al. Exploring virus-host-environment interactions in a chemotrophic-based underground estuary. Environ. Microbiome 19, 9 (2024).

27. Han, Z. & Smith, H. L. Bacteriophage-resistant and bacteriophage-sensitive bacteria in a chemostat. Math. Biosci. Eng. 9, 737–765 (2012).

28. Henry, M., Lavigne, R. & Debarbieux, L. Predicting in vivo efficacy of therapeutic bacteriophages used to treat pulmonary infections. Antimicrob. Agents Chemother. 57, 5961–5968 (2013).

29. Hoeffding, W. A non-parametric test of independence. Ann. Math. Stat. 19, 546–557 (1948).

30. Hunter M., Fusco D. Superinfection exclusion: A viral strategy with short-term benefits and long-term drawbacks. PLoS Comput Biol 18(5): e1010125. (2022)

31. Khan, M. S. I. et al. Bile modulates phage-host interactions in multidrug-resistant *Pseudomonas aeruginosa*. BMC Microbiol. 25, 666 (2025).

32. Kubota, N., Scribner, M. R. & Cooper, V. S. Filamentous cheater phages drive bacterial and phage populations to lower fitness. Curr. Biol. 35, 5220–5229.e3 (2025).

33. Kurilovich, E. & Geva-Zatorsky, N. Effects of bacteriophages on gut microbiome functionality. Gut Microbes 17, 2481178 (2025).

34. Lenski, R. E. & Levin, B. R. Constraints on the coevolution of bacteria and virulent phage: a model, some experiments, and predictions for natural communities. Am. Nat. 125, 585–602 (1985).

35. Levin, B. R., Stewart, F. M. & Chao, L. Resource-limited growth, competition, and predation: a model and experimental studies with bacteria and bacteriophage. Am. Nat. 111, 3–24 (1977).

36. Li, D. et al. Phage-host interaction in *Pseudomonas aeruginosa* clinical isolates with functional and altered quorum sensing systems. Appl. Environ. Microbiol. 91, e02402-24 (2025).

37. Liang, X. et al. Bacteriophage-driven microbial phenotypic heterogeneity: ecological and biogeochemical importance. npj Biofilms Microbiomes 11, 82 (2025).

38. Liu, C., Wang, J., Lei, L., Li, L. & Yuan, X. Gut microbiota therapy for chronic kidney disease. Front. Immunol. 16, 1660226 (2025).

39. Lv, P. et al. Fitness costs of phage-driven resistance mutations in *Salmonella enteritidis* populations. J. Virol. 100, e0195025 (2026).

40. Malik, S., Ahsan, O., Muhammad, K., Munawar, N. & Waheed, Y. Phagetherapy updates: new frontiers against antibiotic resistance. Eur. J. Microbiol. Immunol. 15, 1–12 (2025).

41. McKay, M. D., Beckman, R. J. & Conover, W. J. A comparison of three methods for selecting values of input variables in the analysis of output from a computer code. Technometrics 21, 239–245 (1979).

42. Middelboe, M. Bacterial growth rate and marine virus-host dynamics. Microb. Ecol. 40, 114–124 (2000).

43. Molina, F., Menor-Flores, M. & Vega-Rodríguez, M. A. *SocialViruses*: integrating quantitative phage-bacteria and phage-phage interaction networks for rational cocktail design. Bioinform. Adv. 5, vbaf239 (2025).

44. Molina, F. et al. Diversity and local coadaptation of *Escherichia coli* and coliphages from small ruminants. Front. Microbiol. 11, 1–12 (2020).

45. Monod, J. The growth of bacterial cultures. Annu. Rev. Microbiol. 3, 371–394 (1949).

45. Moon, K. et al. Considerations and perspectives on phage therapy from the transatlantic taskforce on antimicrobial resistance. Nat. Commun. 16, 10883 (2025).

47. Nabergoj, D., Modic, P. & Podgornik, A. Effect of bacterial growth rate on bacteriophage population growth rate. MicrobiologyOpen 7, e00558 (2017).

48. Naderian, R., Alibabaei, F., Paraandavaji, E., Dehghan, P. & Eslami, M. Phage-microbiota interactions in the gut: implications for health and therapeutic strategies. Probiotics Antimicrob. Proteins. doi:10.1007/s12602-025-10784-z. (2025).

49. Nilsson, A. S. Cocktail, a computer program for modelling bacteriophage infection kinetics. Viruses 14, 2483 (2022).

50. Peng, L. et al. Ecological drivers and functional roles of phage communities in the Yangtze River's freshwater ecosystems. J. Hazard. Mater. 500, 140564 (2025).

51. Pottie, I., Vázquez Fernández, R., Van de Wiele, T. & Briers, Y. Phage lysins for intestinal microbiome modulation: current challenges and enabling techniques. Gut Microbes 16, 2387144 (2024).

52. Roughgarden, J. Evolutionarily optimal phage life-history traits: burst size vs. lysis time. bioRxiv 2025.04.16.649164 (2026).

53. Ruan, C., Vinod, D. P. & Johnson, D. R. Phage-mediated peripheral kill-the-winner facilitates the maintenance of costly antibiotic resistance. Nat. Commun. 16, 5839 (2025).

54. Rubio-Portillo, E. et al. Short-term virus-host interactions and functional dynamics in recently deglaciated Antarctic tundra soils. ISME Commun. 5, ycaf157 (2025).

55. Sahoo, K. & Meshram, S. The evolution of phage therapy: a comprehensive review of current applications and future innovations. Cureus (2024). doi:10.7759/cureus.70414.

56. Salehimoghaddam, Z., Hynes, A. P. & Doyle, R. T. From bacterial predators to partners: phages in agriculture. New Phytol. 249, 2729–2735 (2026).

57. Sheraz, M., Shi, H. & Banerjee, S. Human microbiome and bacteriophages: impacts on health and disease. Curr. Genet. Med. Rep. (2025). doi:10.1007/s40588-025-00243-2.

58. Sillankorva, S., Oliveira, R., Vieira, M. J., Sutherland, I. & Azeredo, J. *Pseudomonas fluorescens* infection by bacteriophage ΦS1: the influence of temperature, host growth phase and media. FEMS Microbiol. Lett. 241, 13–20 (2004).

59. Singh, S., Samson, R. & Hassard, F. Phage therapy for environmental biotechnology applications. Front. Microbiol. 16, 1621103 (2025).

60. Šivec, K. & Podgornik, A. Determination of bacteriophage growth parameters under cultivating conditions. Appl. Microbiol. Biotechnol. 104, 8949–8960 (2020).

61. Smith, A., Hunter, M., Bakshi, S. & Fusco, D. Live and let die: lysis time variability and resource limitation shape lytic bacteriophage fitness. PLoS Comput. Biol. 22, e1013340 (2026).

62. Smith, H. L. & Thieme, H. R. Persistence of bacteria and phages in a chemostat. J. Math. Biol. 64, 951–979 (2012).

63. Summers, J. K. & Kreft, J.-U. The role of mathematical modelling in understanding prokaryotic predation. Front. Microbiol. 13, 1037407 (2022).

64. Weitz, J. S. & Dushoff, J. Alternative stable states in host-phage dynamics. Theor. Ecol. 1, 13–19 (2008).

65. Weitz, J. S., Hartman, H. & Levin, S. A. Coevolutionary arms races between bacteria and bacteriophage. Proc. Natl. Acad. Sci. U.S.A. 102, 9535–9540 (2005).

66. Wheatley, R. M., Holtappels, D. & Koskella, B. Evaluation of bacteriophages as a signature of microbiome health: a systematic review and meta-analysis. Lancet Microbe 6, 101196 (2025).

67. Xia, R. et al. Bacterium-phage symbiosis facilitates the enrichment of bacterial pathogens and antibiotic-resistant bacteria in the plastisphere. Environ. Sci. Technol. 59, 2948–2960 (2025).

68. Xing, B. et al. Gut Phage Biobank: a collection of bacteriophages targeting human commensal bacteria. Nat. Commun. 16, 11050 (2025).

69. Ye, J., Meng, Q., Jin, K., Luo, Y. & Yue, T. Phage cocktail alleviated type 2 diabetes by reshaping gut microbiota and decreasing proinflammatory cytokines. Appl. Microbiol. Biotechnol. 108, 1–14 (2024).

Acknowledgements

The author is deeply grateful to Alberto Megias and Santos Bravo Yuste for their help with the simulations.

Funding

This work was supported by the FAGOPORC project, funded by the Ministerio de Agricultura, Pesca y Alimentación (MAPA, Spain) through the AEI-Agri Programme and co-financed by the European Agricultural Fund for Rural Development (EAFRD).

Additional support was provided by Junta de Extremadura through grant GR24046, co-funded (85%) by the European Union through the European Regional Development Fund (ERDF) and by the Spanish Ministry of Finance, acting as Managing Authority.

AI use statement

OpenAI GPT-5.5 was used during manuscript preparation to assist with language editing, text refinement, improvement of manuscript flow, and reference-list formatting. The author reviewed, edited, and approved all AI-assisted modifications and accepts full responsibility for the final content of the manuscript.

Competing interests

The author declares no competing interests.

Additional information

The online version contains supplementary material available at [DOI/URL to be inserted by the publisher].

970

971 **Table 1 Model variables, parameters, and fixed conditions used in the phage–bacteria–**
972 **competitor system.**

State variables and parameters			
Symbol	*Description*	*Range*	*Unit*
H	Total host density ($H = S + R$)	$0–10^{10}$	CFU mL^{-1}
S	Susceptible hosts	$0–10^{10}$	CFU mL^{-1}
I	Infected hosts (tracked implicitly)	$0–10^{10}$	CFU mL^{-1}
R	Resistant hosts	$0–10^{10}$	CFU mL^{-1}
C	Competitor bacteria (non-susceptible)	$0–10^{10}$	CFU mL^{-1}
P	Free phage	$0–10^{10}$	PFU mL^{-1}
ψ_R	Resistant-host growth rate	0–1.5	h^{-1}
μ	Mutation rate to resistance	$10^{-9}–10^{-5}$	cell div. $^{-1}$
ϕ_P	Initial phage density	$10^{2}–10^{7}$	PFU mL^{-1}
σ	Adsorption rate	$10^{-12}–10^{-8}$	mL min^{-1}
ℓ	Latent period	20–60	min
β	Burst size	10–150	PFU $cell^{-1}$
Fixed conditions			
Symbol	*Description*	*Value*	*Unit*
K	Half-saturation constant (Monod)	5.0	µg mL^{-1}
ψ_S	Susceptible-host growth rate	1.0	h^{-1}
ψ_C	Competitor growth rate	0.75	h^{-1}
ϕ_S	Initial susceptible host density	10^{6}	CFU mL^{-1}
ϕ_C	Initial competitor density	1	CFU mL^{-1}
ϕ_R	Initial resistant-host density	0	CFU mL^{-1}
N_0	Initial nutrient concentration	100	µg mL^{-1}
N_{in}	Inflow nutrient concentration	100	µg mL^{-1}
ω	Dilution (flow) rate	0.2	h^{-1}
ε	Nutrient conversion coefficient	2×10^{-6}	µg $cell^{-1}$

973

Supplementary Files

This is a list of supplementary files associated with this preprint. Click to download.

- SupplementaryInformationrevisedclean.docx